SCIEPublish

Article

Direct-Ink-Writing Printing of Shape Memory Cross-Linked Networks from Biomass-Derived Small Molecules

Dan Liu, Di Wu, Yi Xiao, Rui Zhan, Xin-Rong Zeng and Ke-Ke Yang *

The Collaborative Innovation Center for Eco-Friendly and Fire-Safety Polymeric Materials (MoE), National Engineering Laboratory of Eco-Friendly Polymeric Materials (Sichuan), State Key Laboratory of Polymer Materials Engineering, College of Chemistry, Sichuan University, Chengdu 610064, China; 1097088853@qq.com (D.L.); 1346990135@qq.com (D.W.); xiaoyi@stu.scu.edu.cn (Y.X.); m19942331358@163.com (R.Z.); zxr18997@163.com (X.-R.Z.)

* Corresponding author. E-mail: kkyang@scu.edu.cn (K.-K.Y.)

Received: 29 July 2024; Accepted: 14 September 2024; Available online: 18 September 2024

ABSTRACT: The rapid development of 3D printing, also known as additive manufacturing, has opened up new opportunities for applying shape memory polymers (SMPs) in various fields. The use of abundant, inexpensive, and easily accessible biomass materials as printing raw materials not only facilitates the creation of more intricate SMPs but also aligns with the principles of low-carbon, green, and sustainable development. Here, we successfully printed a shape memory cross-linked network (NW-MO-TTMP) in a single step by direct-ink-writing printing and an *in-situ* thiol-ene click reaction with magnolol and trimethylolpropane tris(3-mercaptopropionate) as raw materials. The resulting NW-MO-TTMP network exhibited high mechanical properties and a tensile strength (σ) of up to 2.7 MPa when the thiol-ene ratio was 1.0:1, and the photo-initiator content was 1.5%. To improve printability, ethyl cellulose (EC) derived from biomass was incorporated to enhance the viscosity of the printing precursor fluid, resulting in a significant increase in the σ of the NW-MO-TTMP/EC network, reaching 20.6 MPa. Moreover, the successful printing of intricate models, such as the 'whale' and 'octopus,' demonstrated excellent shape memory effects. This approach highlights the potential of combining biomass-derived materials with advanced 3D printing techniques to develop sustainable and high-performance SMPs.

Keywords: Direct-ink-writing printing; Shape memory; Thiol-ene click reaction; Biobased materials

1. Introduction

Shape memory polymers (SMPs) are intelligent adaptive materials that can be programmed from an initial shape to a temporary shape under certain conditions and then revert to their initial shape under external stimuli such as light, heat, electricity, magnetism, etc. [1–5]. SMPs have found applications in various fields, including biomedicine [6–8], electronic devices [9,10], and aerospace [11,12]. However, as the complexity and customization of specific requirements continue to evolve, traditional processing methods like injection molding and blow molding face challenges in meeting the further advancements of SMPs.

In recent years, additive manufacturing (3D printing) has emerged as a new processing method that offers advantages such as the efficient use of raw materials, and the ability to create personalized and intricate three-dimensional structures [13–15], which greatly expand the application fields of SMPs. Among various 3D printing techniques, extrusion printing, e.g., fused-deposition-modeling printing (FDM) and direct-ink-writing (DIW), stands out as it enables direct extrusion from the nozzle head, depositing and solidifying them layer by layer. It has gained popularity due to its simplicity, feasibility, and cost-effectiveness. DIW demonstrates remarkable versatility, enabling the use of a wide range of raw materials, such as small molecule compounds, polymers, hydrogels, ceramics, metals, and even living cells [16–19]. To meet the rheological requirements for extrusion, viscous inks are often shear-thinning and require post-processing, such as curing, to solidify.Thus, rheological modifiers and ultraviolet (UV) assistance are commonly employed in DIW printing [20–22]. These advantages provide great convenience for producing SMPs with complex 3D architecture from linear polymers and reactive precursors [23]. For example, Wan et al. utilized poly(D, L-

https://doi.org/10.70322/spe.2024.10008

Lactide-co-trimethycarbonate) as the printing material, dissolving it in dichloromethane to prepare DIW printing ink by adjusting the concentration. Concurrently, the printing and solvent evaporation rate were modulated to facilitate the printing of SMPs, which can be applied in minimally invasive fields [24]. Roach et al. utilized nano-clay as a viscosity modifier to formulate DIW inks, facilitating room temperature DIW printing of long liquid crystal elastomer (LCE) fibers. Single-domain LCE fibers were synthesized using a two-step method, demonstrating reversible actuation of up to 51%. This LCE exhibits significant potential for applications in smart clothing, soft robotics, and biomedical devices [25].

Utilizing biomass-derived resources, such as natural polymers, as printing raw materials contributes to the green and sustainable development of polymer materials [26–28]. Examples of these thermoplastic biomass materials include polylactic acid, polybutylene succinate, and cellulose [29–31]. DIW printing offers the feasibility of conducting polymerization and molding from photosensitive biomass-derived small molecules in one step. Rodriguez et al. developed printable ink using renewable epoxy soybean oil small molecules with carbon nanofibers for heat-cured DIW printing, demonstrating electrical response properties [32]. Nevertheless, this printed material presents certain drawbacks, including the fragility of products formed from acrylic esters and the slow curing speed associated with epoxy raw materials.

Leveraging the versatility and high efficiency of DIW, herein, we fabricated a series of biobased shape memory cross-linking networks via a UV-initiated thiol-ene click reaction of well-prepared inks. The printing inks are mainly composed of unsaturated biomass-derived small molecules and mercaptan crosslinkers, and the structures of these two components were screened based on the mechanical performance of the resulting networks. Furthermore, ethyl cellulose (EC) was introduced to enhance the viscosity of the printing inks, facilitating the printing and improving the mechanical properties of the resulting network. An optimized sample, NW-MO-TTMP/EC$^{20\%}$, exhibited a high tensile strength (σ) of 20.6 MPa. Additionally, the excellent SMEs of NW-MO-TTMP/EC networks were demonstrated, with an R_f exceeding 99.7% and an R_r exceeding 98.6%. Based on the NW-MO-TTMP/EC$^{20\%}$, shape memory 'whale' and 'squid' models were successfully printed with optimized printing parameters.

2. Materials and Methods

2.1. Materials

Magnolol (MO) was purchased from Adamas (Shanghai, China). Trimethylolpropane tris(3-mercaptopropionate) (TTMP), cinene (NE), and ethyl cellulose (EC) were supplied by TCI (Shanghai, China). Phenylbis(2,4,6-trimethylbenzoyl) phosphine oxide (BAPO), and castor oil (CSO) were provided by Aladdin (Shanghai, China). 3,6-Dioxa-1,8-octanedithiol (DODT) was supported by Shanghai Hao Hong Biological Medicine Technology Co., Ltd. (Shanghai, China). Dichloromethane (DCM) was provided by Zhiyuan Chemical Co., Ltd. (Tianjin, China). All materials and reagents were used without further purification.

2.2. Preparation of Bio-Based Cross-Linked Networks Via UV-Initiated Thiol-Ene Reaction

A specific quantity of biobased monomer, mercaptan crosslinker, and photo-initiator BAPO were added into a reaction bottle. An equal volume of DCM solvent was added, and the mixture was stirred at room temperature until all materials dissolved. The reaction bottle was covered with aluminum foil during the dissolution process to avoid interference from ambient UV light. Once the solution turned into a clear yellow liquid, a syringe is used to transfer the solvent mixture into a sandwich-type glass mold. A UV lamp was positioned at a specific height, and both sides of the glass plates were exposed to light for 5s each. The setup was removed to allow the solvent to evaporate. Finally, the film was dried at 60 °C in an oven until a constant weight was achieved.

2.3. Preparation of Printing Precursor Liquid

MO, TTMP, BAPO, and an appropriate amount of EC were added to a weighing bottle. The mixture was dissolved in DCM until it formed a yellow transparent viscous liquid and was allowed to stand to eliminate bubbles generated during stirring. It is crucial to shield the solution from light during the dissolution process. Note that x in the NW-MO-TTMP/EC^x cross-linked network represents the mass fraction of EC.

2.4. UV-Assisted DIW Printing

A Dr. INVIVO.4D (Seoul, Korea) printer was employed for UV-DIW printing. The print model structure was first constructed and its .stl file was imported into the printer's slicing software (NewCreator K, Version 1.57.80). The resulting sliced data in g-code format was imported into the printer. Then, the printhead equipped with a UV lamp was

selected, and the parameters were adjusted as follows: 0.6 mm nozzle diameter, 0.48 mm print height (50–80% of the nozzle diameter), linear infill pattern, printing speed of 7 mm/s, and infill density of 45%. After the position calibration, the bio-inks were added to the syringe to start the printing. The UV intensity range varied under different printer areas, ranging from 6 to 24 mW/cm^2.

2.5. Structure Characterization and Performance Testing Methods

Differential Scanning Calorimetry (DSC) was performed with a DSC-Q200 (TA Instrument, New Castle, DE, USA) over the temperature range from −60 to 40 °C at a heating (or cooling) rate of 10 °C·min^{-1} under a steady flow of ultra-high-purity nitrogen purge and empty aluminum as the reference. Mechanical tests were conducted using an Instron Universal Testing Machine (SANS CMT4104, SANS Group, Shanghai, China) at a loading speed of 0.17 m·s^{-1} and a temperature of 25 °C. The samples used were dumbbell-shaped with dimensions of 50 mm length × 4 mm width × 0.5 mm thickness and the data was collected by averaging results from multiple specimens. The other details of characterization are provided in Supporting Information.

3. Results and Discussion

3.1. Preparation of Cross-Linked Networks from Biomass-Derived Small Molecules

In our study, aiming for environmental sustainability, we developed biobased shape memory networks with desirable mechanical properties and SMEs using DIW printing technology directly from biomass-derived small molecules with reactive double bonds.

To ensure rapid curing of small molecules during DIW printing, mercaptan compounds were used as crosslinkers to initiate the thiol-ene click reaction.

To create a cross-linking network with desirable comprehensive performance, different mercaptan crosslinkers (TTMP and DODT) and biomass-derived small molecules with different rigidities and double-bond contents (CSO, NE, and MO) were screened (Figure 1a).

Firstly, CSO with flexible fatty chains was selected as a double-bond donor to react with mercaptan crosslinkers TTMP and DODT, resulting in cross-linking networks NW-CSO-TTMP and NW-CSO-DODT, respectively (see the details of feed ratios in Table S1). The mechanical performance of the resulting networks was evaluated, with the stress-strain curves shown in Figure 1b and relevant data provided in Table S1. NW-CSO-TTMP using TTMP exhibited a σ of 0.8 MPa and an elongation at break (ε) of 49%, much higher than the NW-CSO-DODT network, which had a σ of 0.4 MPa. The superior performance of NW-CSO-TTMP can be attributed to the trifunctional sulfhydryl groups in TTMP, which lead to a higher cross-linking density. Additionally, the presence of ester bonds facilitates the formation of hydrogen bonds, further enhancing the material's mechanical properties. Therefore, TTMP was chosen as a crosslinker in further investigation.

In addition to the crosslinker, the structure of the biobased small molecule is crucial in determining the comprehensive performance of the resulting network. Alongside CSO containing long flexible fatty chains, NE with an aliphatic ring and MO with an aromatic ring (Figure 1a) were also chosen to react with TTMP. The mechanical properties of resulting networks were evaluated, with stress-strain curves shown in Figure 1c and the corresponding data provided in Table S1. All the samples exhibited typical elastomer tensile curve characteristics without yielding. The NW-NE-TTMP cross-linked network demonstrated a σ of 0.7 MPa and ε of 50%. In contrast, the NW-MO-TTMP network showed significantly enhanced mechanical properties, with a σ of 2.7 MPa and an ε of 378%, as shown in Figure 1d. This improvement can be attributed to the biphenyl structure in MO, which imparts a degree of rigidity and increases intermolecular forces due to its symmetry. Therefore, combining MO with TTMP creates a bio-based shape memory network with enhanced mechanical properties, highlighting the potential of using biomass-derived small molecules in advanced DIW printing applications.

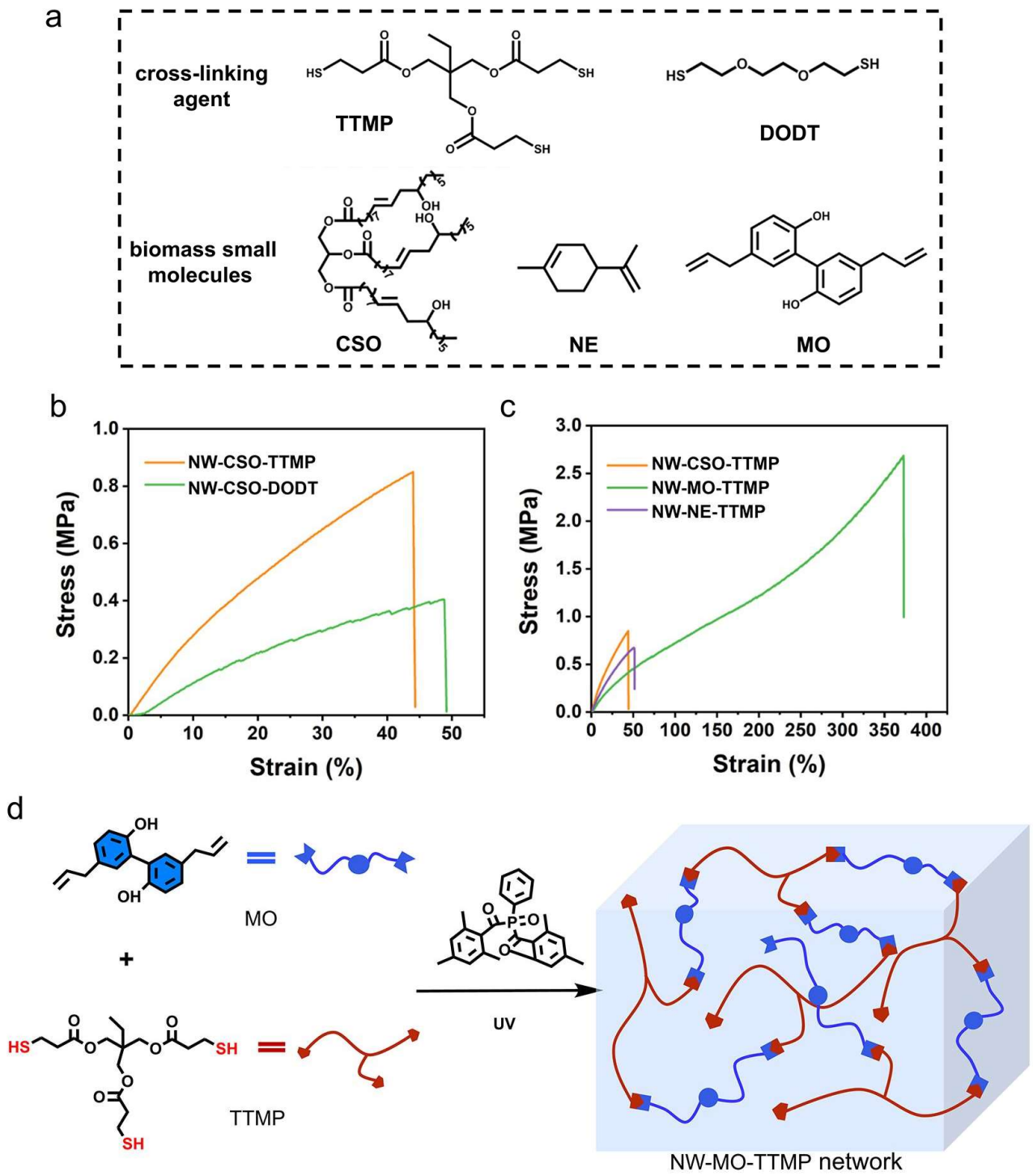

Figure 1. (**a**) Chemical structure of cross-linking agent and biomass-derived small molecules; Stress-strain curves of elastomers with different crosslinkers (**b**) and different biomass-derived small molecules (**c**); (**d**) reaction diagram of NW-MO-TTMP cross-linked network.

3.2. Optimization of Cross-Linking Conditions

After determining the main components for the precursor inks, the feed ratios, including the ratio of thiol-ene (r), concentration (c), the mass fraction of BAPO (w_{BAPO}), and the curing conditions, e.g., the printing power of UV lamp (P), were also optimized. UV-assisted dynamic rheological experiments on precursor inks with varying compositions and swelling tests were performed to assess the cross-linking degree after 5 s of illumination (Table S2). The rheological curves indicate that the inks with different compositions initially behave as liquids, exhibiting a storage modulus (G') that is lower than the loss modulus (G"). As the reaction time extends, the inks gradually underwent gelation, resulting in G' surpassing G". This phenomenon suggests that the ink can be cured under UV light, facilitating the smooth printing of DIW. Based on the swelling test and the dynamic rheological behaviors (as shown in Table S2 and Figures 2 and

S1–S4), the optimized parameters and conditions were confirmed as: r = 1, c = 1.5 g/mL, w_{BAPO} = 1.5%, and P = 20 mW/cm². Under these conditions, the G value of the cross-linking network reaches 91.8%, indicating a favorable cross-linking density that supports a desirable SME of the network.

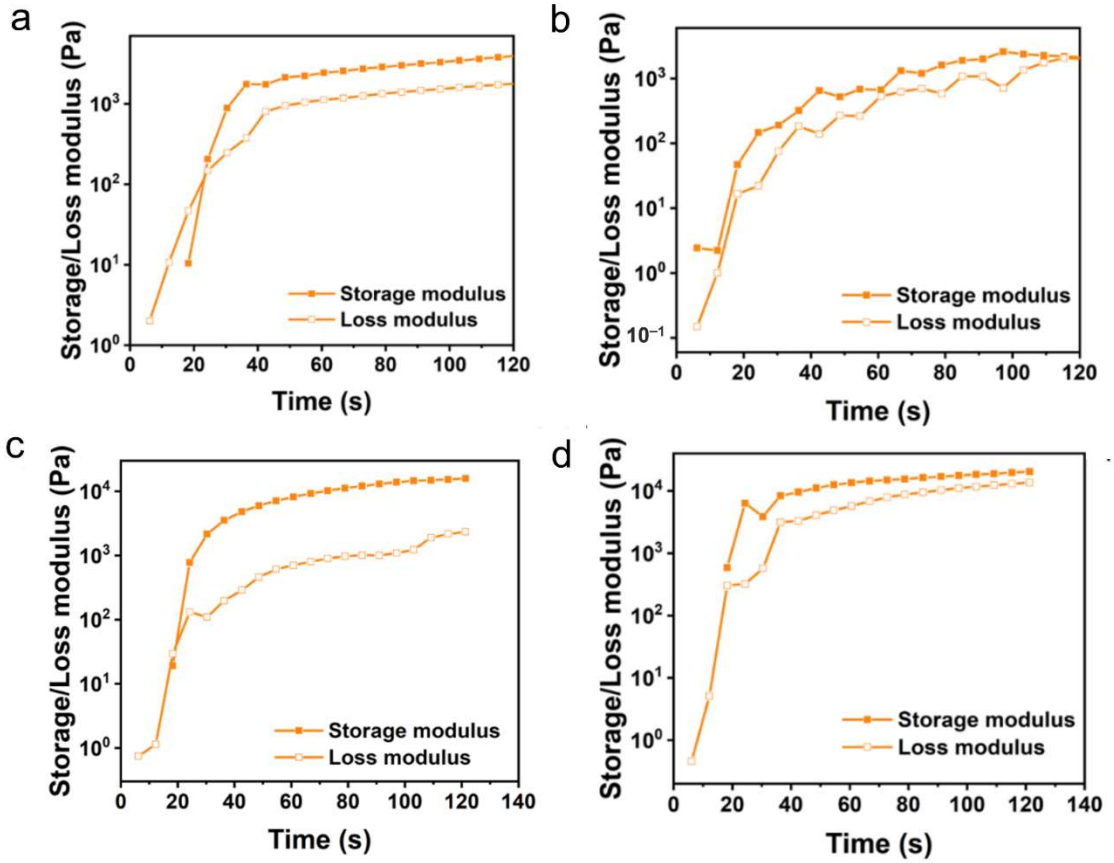

Figure 2. UV-assisted dynamic rheological testing of MO-TTMP with different conditions: different ratios of r = 0.8 (**a**); r = 1.0 (**b**) (P = 30 mW/cm²; c = 1.5 g/mL; w_{BAPO} = 2.0%); (**c**) r = 1, P = 30 mW/cm², c = 1.5 g/mL, w_{BAPO} = 1.5%; (**d**) r = 1, P = 20 mW/cm², c = 1.5 g/mL, w_{BAPO} = 1.5%.

3.3. Preparation of NW-MO-TTMP/EC

Although NM-MO-TTMP was prepared under optimized components and UV cross-linking parameters, there remained the challenge with the low viscosity of the precursor ink, which made it hard to extrude continuously and cured rapidly even with UV irradiation. To address this issue, EC, a small molecule derived from biomass, was added as a thickener due to its excellent solubility in DCM and its numerous hydrogen bond interactions within its structure.

The viscosities of precursor inks with varying mass fractions of EC (w_{EC}) were analyzed through steady-state shear experiments. Figure 3a shows that with the w_{EC} increased, the initial viscosities of the inks increased from 7 Pa·s to 58 Pa·s. All inks showed a shear thinning behavior, which is beneficial for DIW printing. Adequate thixotropic behavior of inks is also required to maintain a certain level of shape retention before curing. Thus, the printability of inks with different w_{EC} was evaluated by analyzing their modulus in cyclic strains at 1% and 1000% (Figure 3b–e). A 1% strain represents the state of the ink in the cylinder without external force, while a 1000% strain simulates external extrusion. The increase in w_{EC} increased hydrogen bonds within the system, leading to a gradual rise in the modulus. Furthermore, at high strains, the G' and G" values of MO-TTMP/EC decreased, consistent with its 'shear thinning' behavior, facilitating smooth flow from the needle and rapid return to the initial state after extrusion removal, assisting in shape preservation post-printing.

The impact of w_{EC} on the cross-linking degree and the mechanical properties of NW-MO-TTMP/ECs was investigated. The swelling data in Table S3 indicate that EC does not significantly affect the cross-linking degree of the networks, with G remaining at around 95% and S at approximately 300%. The stress-strain curves of NW-MO-TTMP/ECs are illustrated in Figure 3f, with corresponding data detailed in Table S3. It is evident that with the increase of w_{EC} from 9% to 20%, the σ of NW-MO-TTMP/ECs notably increased from 9.4 MPa to 20.6 MPa, while ε decreases from 383% to 229%. This change is attributed to the network's augmented number of hydrogen bonds.

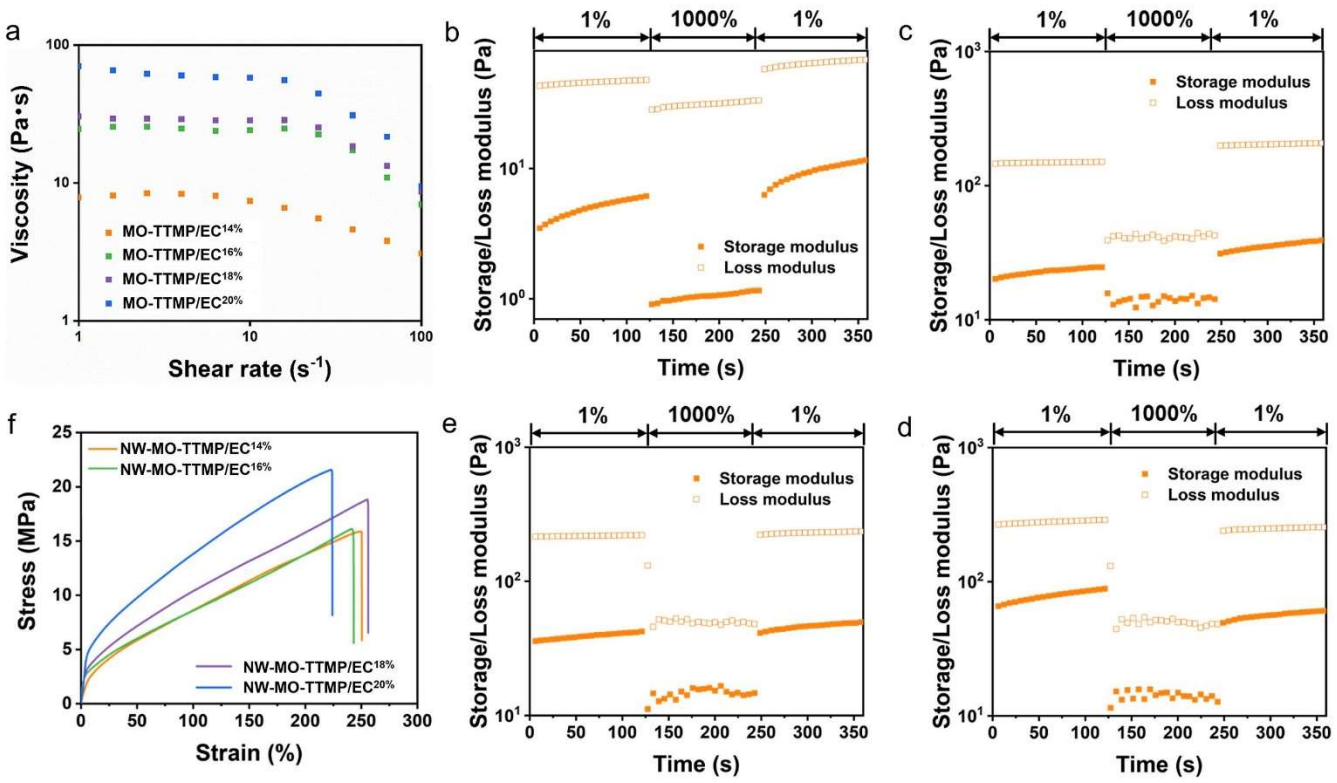

Figure 3. (**a**) Viscosity of MO-TTMP/EC as a function of shear rate with different EC contents; Storage modulus and loss modulus of MO-TTMP/EC as a function of shear strain with different EC contents: MO-TTMP/EC$^{14\%}$ (**b**); MO-TTMP/EC$^{16\%}$ (**c**); MO-TTMP/EC$^{18\%}$ (**d**); MO-TTMP/EC$^{20\%}$ (**e**); (**f**) Stress-strain curves of NW-MO-TTMP with different EC contents.

3.4. Shape Memory Effects of NW-MO-TTMP/EC

Before investingating the SMEs of NW-MO-TTMP/ECs, the thermal properties of NW-MO-TTMP/ECs were first analyzed (Figure S5). The analysis revealed that the glass transition temperature (T_g) slightly increased with higher w_{EC}, e.g., from 9.7 °C for NW-MO-TTMP/EC$^{14\%}$ to 13.2 °C for NW-MO-TTMP/EC$^{20\%}$. This increase in T_g can be attributed to the hydrogen bond interactions introduced by EC, which restricted the movement of molecular chain segments. The T_gs of the NW-MO-TTMP/ECs, being slightly lower than room temperature, were employed as the shape memory transition temperatures during the SME cycles. The thermo-mechanical cyclic tests were conducted to quantitatively evaluate the SMEs of NW-MO-TTMP/ECs, with results shown in Figure 4 and corresponding data provided in Table S4. Interestingly, w_{EC} did not significantly impact the SMEs of NW-MO-TTMP/EC samples, as all networks displayed excellent shape memory properties, with R_f values exceeding 99.7% and R_r values surpassing 98.6%. Compared to other DIW-based materials, our synthesized material offers several advantages. In addition to using biomass monomers as raw materials, it offers significantly faster curing times compared to epoxy-based composites, which typically require over 2 h for full curing [32]. Additionally, unlike hydrogels formulated from acrylates [33,34], our approach eliminates the need for post-processing steps. The printing process is simple and efficient, with no need for additional treatments, such as soaking, to improve the network structure.

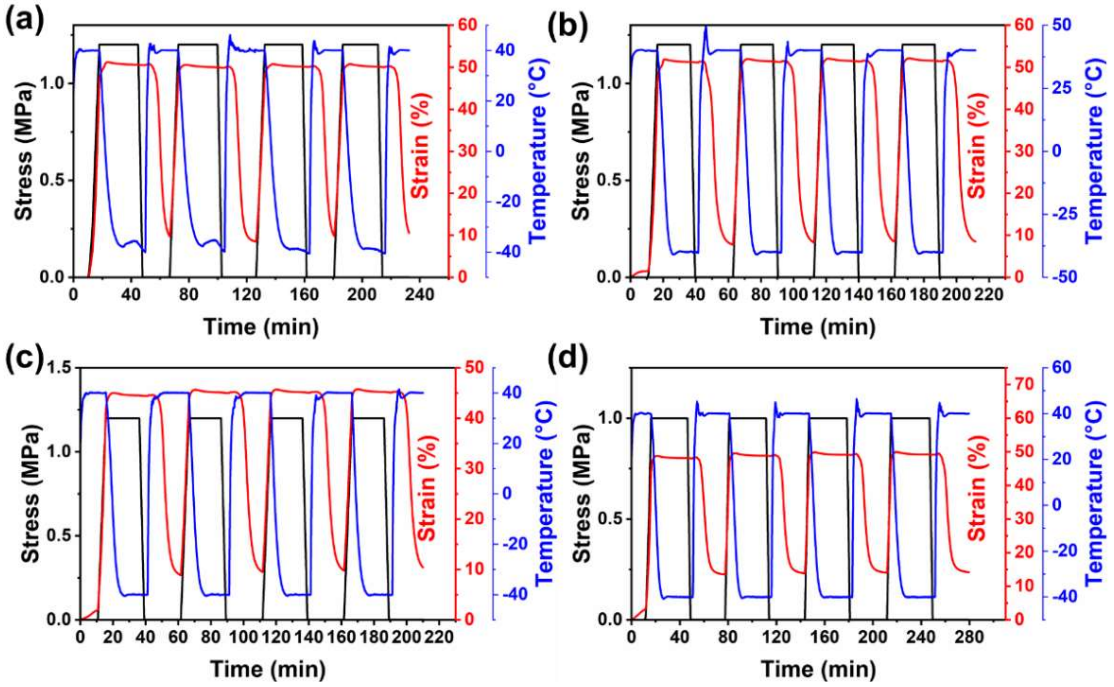

Figure 4. SMEs of NW-MO-TTMP/EC recorded from the cyclic thermal mechanical tests: MO-TTMP/EC$^{14\%}$ (**a**); MO-TTMP/EC$^{16\%}$ (**b**); MO-TTMP/EC$^{18\%}$ (**c**); MO-TTMP/EC$^{20\%}$ (**d**).

3.5. UV-DIW Printing of MO-TTMP/EC

Given the excellent comprehensive performance of NW-MO-TTMP/EC$^{20\%}$, its corresponding inks MO-TTMP/EC$^{20\%}$ were used to print 'whale' and 'octopus' models (Figure 5). These print models were programmed to showcase their shape memory performance. In Figure 5a, the oscillating state of the 'whale' tail is simulated; it was programmed at room temperature in the direction of the arrow first, its temporary shape was fixed at 0 °C, and it gradually returned to its original shape at room temperature. Similarly, Figure 5b demonstrates the changes in the antennae of the 'octopus,' confirming the excellent SME of MO-TTMP/EC$^{20\%}$ samples produced by UV-DIW.

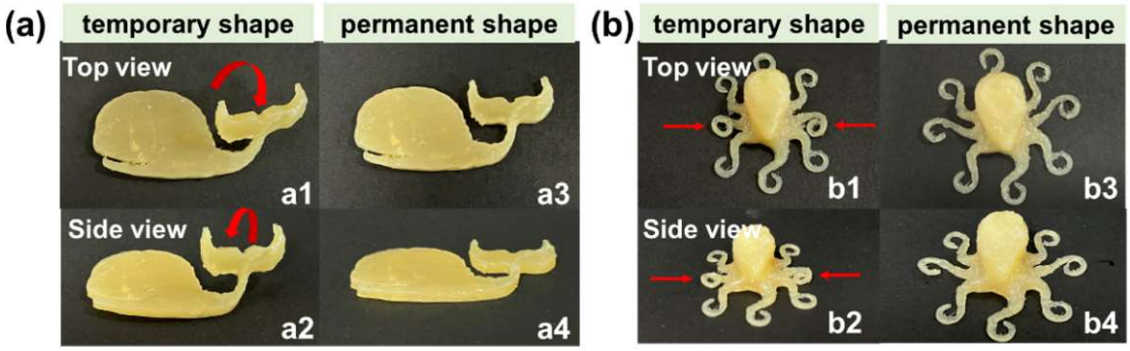

Figure 5. Thermal-introduced shape memory processes of the 'whale' (**a**) and the 'octopus' (**b**) from the top and side view: (**a1**,**a2**,**b1**,**b2**) temporary shape fixed at 0 °C; (**a3**,**a4**,**b3**,**b4**) permanent shape recovered at room temperature.

4. Conclusions

This study explores the direct synthesis of shape memory cross-linking networks using biomass-derived unsaturated small molecules and mercaptan crosslinkers through UV-triggered thiol-ene click reactions. A biomass-derived EC thickener was introduced to enhance the viscosity of the printing inks and improve mechanical performance. The different crosslinkers and biomass-derived unsaturated small molecules were selected to prepare precursor inks. Tensile tests revealed that the combination of MO and TTMP exhibits the best performance. The incorporation of EC significantly increased the viscosities of the precursor inks, as demonstrated by steady-state shear tests. Oscillatory shear tests indicated that higher EC content leads to a significant increase in *G'*, helping maintain the shape of the extruded precursor inks. Increasing w_{EC} resulted in the pronounced reinforcement effect,achieving a σ of 20.6 MPa.

DMA test results demonstrate that NW-MO-TTMP/EC networks displayed excellent SME, with R_f above 99.7% and R_r reaching 98.6% for all networks. Successful DIW printing of 'whale' and 'octopus' MO-TTMP/EC$^{20\%}$ models was demonstrated with desirable SME. These findings highlight the successful development and application of biobased shape memory networks through UV-DIW 4D printing, paving the way for future research and practical applications in this field.

Supplementary Materials

The following supporting information can be found at: https://www.sciepublish.com/article/pii/280, Figure S1: UV-assisted dynamic rheological testing of MO-TTMP with different *r*. Figure S2: UV-assisted dynamic rheological testing of MO-TTMP with different *c*. Figure S3: UV-assisted dynamic rheological testing of MO-TTMP with different w_{BAPO}. Figure S4:UV-assisted dynamic rheological testing of MO-TTMP with different *P*. Figure S5: DSC curves of NW-MO-TTMP/EC. Table S1: Tensile relevant data of elastomers with different crosslinkers and biomass-derived unsaturated small molecules. Table S2: Tensile and swelling data of NW-MO-TTMP with different *r*, *c*, w_{BAPO} and *P*. Table S3: The data of tensile and swelling tests of NW-MO-TTMP/ECs. Table S4: DSC and SMEs data of NW-MO-TTMP/EC.

Acknowledgments

The authors thanks Dr. Hui Xie from Southwest Jiaotong University for his valuable suggestion on the printing.

Author Contributions

Conceptualization, D.W. and K.-K.Y.; Methodology, D.L. and D.W.; Validation, D.W., D.L.,Y.X. and R.Z. Investigation, D.W. and X.-R.Z.; Data Curation, D.W.; Writing—Original Draft Preparation, D.L.; Writing—Review & Editing, K.-K.Y.; Visualization, D.W. and D.L.; Supervision, K.-K.Y.; Project Administration, K.-K.Y.; Funding Acquisition, K.-K.Y.

Ethics Statement

Not applicable.

Informed Consent Statement

Not applicable.

Funding

This work was financially supported by the National Key Research and Development Program of China (2022YFC2104600/2022YFC2104604).

Declaration of Competing Interest

The authors declare that they have no known competing financial interests or personal relationships that could have appeared to influence the work reported in this paper.

References

1. Lendlein A, Kelch S. Shape-Memory Polymers. *Angew. Chem. Int. Ed*. **2002**, *41*, 2034–2057.
2. Yue CB, Li M, Liu YT, Fang YQ, Song YM, Xu M, et al. Three-Dimensional Printing of Cellulose Nanofibers Reinforced PHB/PCL/Fe_3O_4 Magneto-Responsive Shape Memory Polymer Composites with Excellent Mechanical Properties. *Addit. Manuf.* **2021**, *46*, 102146.
3. Wei Y, Huang R, Dong P, Qi XD, Fu Q. Preparation of Polylactide/Poly(ether)urethane Blends with Excellent Electro-actuated Shape Memory via Incorporating Carbon Black and Carbon Nanotubes Hybrids Fillers. *Chin. J. Polym. Sci.* **2018**, *36*, 1175–1186.
4. Xie T. Tunable Polymer Multi-Shape Memory Effect. *Nature* **2010**, *464*, 267–270.
5. Hofmann A, Hauptmann M. Ultrasonic Induced Material Compression During the Gap-controlled Reshaping of Dry Paper Webs by Embossing or Deep Drawing. *Bioresources* **2020**, *15*, 2326–2338.
6. Lin C, Liu LW, Liu YJ, Leng JS. 4D Printing of Bioinspired Absorbable Left Atrial Appendage Occluders: A Proof-of-Concept Study. *ACS Appl. Mater. Interfaces* **2021**, *13*, 12668–12678.

7. Langford T, Mohammed A, Essa K, Elshaer A, Hassanin H. 4D Printing of Origami Structures for Minimally Invasive Surgeries Using Functional Scaffold. *Appl. Sci.* **2021**, *11*, 332.
8. Lin C, Lv JX, Li YS, Zhang FH, Li JR, Liu YJ, et al. 4D-Printed Biodegradable and Remotely Controllable Shape Memory Occlusion Devices. *Adv. Funct. Mater*. **2019**, *29*, 1906569.
9. Deng DP, Jain A, Yodvanich N, Araujo A, Chen Y. Three-Dimensional Circuit Fabrication Using Four-Dimensional Printing and Direct Ink Writing. In Proceedings of the 2016 International Symposium on Flexible Automation (ISFA), Cleveland, OH, USA, 1–3 August 2016; pp. 286–291.
10. Zarek M, Layani M, Cooperstein I, Sachyani E, Cohn D, Magdassi S. 3D Printing of Shape Memory Polymers for Flexible Electronic Devices. *Adv. Mater.* **2016**, *28*, 4449–4454.
11. Tan Q, Li FF, Liu LW, Liu YJ, Yan XQ, Leng JS. Study of Low Earth Orbit Ultraviolet Radiation and Vacuum Thermal Cycling Environment Effects on Epoxy-Based Shape Memory Polymer. *J. Intell. Mater. Syst. Struct*. **2019**, *30*, 2688–2696.
12. Lee KM, Koerner H, Vaia RA, Bunning TJ, White TJ. Light-Activated Shape Memory of Glassy, Azobenzene Liquid Crystalline Polymer Networks. *Soft Matter* **2011**, *7*, 4318–4324.
13. Khoo ZX, Teoh JEM, Yong L, Kai CC, Shoufeng Y, Jia A, et al. 3D Printing of Smart Materials: A Review on Recent Progresses in 4D Printing. *Virtual Phys. Prototyp.* **2015**, *10*, 103–122.
14. Momeni F, Sabzpoushan S, Valizadeh R, Morad MR, Liu X, Ni J. Plant Leaf-Mimetic Smart Wind Turbine Blades by 4D Printing. *Renew. Energy* **2019**, *130*, 329–351.
15. Bakarich SE, Gorkin R, Panhuis MIH, Spinks GM. 4D Printing with Mechanically Robust, Thermally Actuating Hydrogels. Macromol. *Rapid Commun*. **2015**, *36*, 1211–1217.
16. Wegst UGK, Bai H, Saiz E, Tomsia AP, Ritchie RO. Bioinspired Structural Materials. *Nat. Mater.* **2015**, *14*, 23–36.
17. Zhu C, Han TYJ, Duoss EB, Golobic AM, Kuntz JD, Spadaccini CM, et al. Highly Compressible 3D Periodic Graphene Aerogel Microlattices. *Nat. Commun.* **2015**, *6*, 6962.
18. Compton BG, Lewis JA. 3D-Printing of Lightweight Cellular Composites. *Adv. Mater*. **2014**, *26*, 5930–5935.
19. Li XT, Zhang P, Li Q, Wang HR, Yang CH. Direct-Ink-Write Printing of Hydrogels Using Dilute Inks. *ISCICE* **2021**, *24*, 102319.
20. Chen KJ, Kuang X, Li V, Kang GZ, Qi HJ. Fabrication of Tough Epoxy with Shape Memory Effects by UV-Assisted Direct-Ink Write Printing. *Soft Matter* **2018**, *14*, 1879–1886.
21. Kotikian A, Truby RL, Boley JW, White TJ, Lewis JA. 3D Printing of Liquid Crystal Elastomeric Actuators with Spatially Programed Nematic Order. *Adv. Mater*. **2018**, *30*, 1706164.
22. Kim Y, Yuk H, Zhao RK, Chester SA, Zhao XH. Printing Ferromagnetic Domains for Untethered Fast-Transforming Soft Materials. *Nature* **2018**, *558*, 274–279.
23. Tibbits S. 4D Printing: Multi-Material Shape Change. *Archit. Des.* **2014**, *84*, 116–121.
24. Wan X, Wei HQ, Zhang FH, Liu YJ, Leng JS. 3D printing of Shape Memory Poly(d,l-Lactide-co-Trimethylene Carbonate) by Direct Ink Writing for Shape-Changing Structures. *J. Appl. Polym. Sci.* **2019**, *136*, 48177.
25. Roach DJ, Yuan C, Kuang X, Li VCF, Blake P, Romero ML, et al. Long Liquid Crystal Elastomer Fibers with Large Reversible Actuation Strains for Smart Textiles and Artificial Muscles. *ACS Appl. Mater. Interfaces* **2019**, *11*, 19514–19521.
26. Schutyser MAI, Houlder S, de Wit M, Buijsse CAP, Alting AC. Fused Deposition Modelling of Sodium Caseinate Dispersions. *J. Food Eng*. **2018**, *220*, 49–55.
27. Siqueira G, Kokkinis D, Libanori R, Hausmann MK, Gladman AS, Neels A, et al. Cellulose Nanocrystal Inks for 3D Printing of Textured Cellular Architectures. *Adv. Funct. Mater*. **2017**, *27*, 1604619.
28. Joe J, Shin J, Choi YS, Hwang JH, Kim SH, Han J, et al. A 4D Printable Shape Memory Vitrimer with Repairability and Recyclability through Network Architecture Tailoring from Commercial Poly(ε-Caprolactone). *Adv. Sci.* **2021**, *8*, 2103682.
29. Muñoz J, Pumera M. 3D-Printed COVID-19 Immunosensors with Electronic Readout. *Chem. Eng. J*. **2021**, *425*, 131433.
30. Yue CB, Hua MQ, Li HQ, Liu YT, Xu M, Song YM. Printability, Shape-Memory, and Mechanical Properties of PHB/PCL/CNFs Composites. *J. Appl. Polym. Sci.* **2021**, *138*, 50510.
31. Hu X, Zhao W, Zhang Z, Xie J, He J, Cao J, et al. Novel 3D Printed Shape-Memory PLLA-TMC/GA-TMC Scaffolds for Bone Tissue Engineering with the Improved Mechanical Properties and Degradability. *Chin. Chem. Lett*. **2023**, *34*, 107451.
32. Rodriguez JN, Zhu C, Duoss EB, Wilson TS, Spadaccini CM, Lewicki JP. Shape-Morphing Composites with Designed Micro-Architectures. *Sci. Rep.* **2016**, *6*, 27933.
33. Imrie P, Diegel O, Jin J. Direct-Ink-Write 3D Printing of "Living" Polymer Hydrogels via Type I Photoinitiated RAFT Polymerization. *Polymer* **2023**, *276*, 125944.
34. Liu J, Erol O, Pantula A, Liu W, Jiang Z, Kobayashi K, et al. Dual-Gel 4D Printing of Bioinspired Tubes. ACS Appl. Mater. Interfaces **2019**, *11*, 8492–8498.